PCCP

Dynamic Article Links

Cite this: *Phys. Chem. Chem. Phys.*, 2011, **13**, 14235–14242

www.rsc.org/pccp

PAPER

Infrared and microwave spectra of the acetylene–ammonia and carbonyl sulfide–ammonia complexes: a comparative study of a weak C–H···N hydrogen bond and an S···N bond†

Xunchen Liu and Yunjie Xu*

Received 13th May 2011, Accepted 29th June 2011
DOI: 10.1039/c1cp21554j

We report a combined high resolution infrared and microwave spectroscopic investigation of the acetylene–ammonia and carbonyl sulfide–ammonia complexes using a pulsed slit-nozzle multipass absorption spectrometer based on a quantum cascade laser and a pulsed nozzle beam Fourier transform microwave spectrometer, respectively. The ro-vibrational transitions of the acetylene–ammonia complex have been measured at 6 μm in the vicinity of the ν_4 band of ammonia for the first time. The previously reported pure rotational transitions have been extended to higher J and K values with ^{14}N nuclear quadrupole hyperfine components detected and analyzed. The spectral analysis reveals that acetylene binds to ammonia through a C–H···N weak hydrogen bond to form a C_{3v} symmetric top, consistent with the previous microwave [Fraser *et al.*, *J. Chem. Phys.*, 1984, **80**, 1423] and infrared spectroscopic study at 3 μm [Hilpert *et al.*, *J. Chem. Phys.*, 1996, **105**, 6183]. A parallel study has also been carried out for the carbonyl sulfide–ammonia complex whose pure rotational and ro-vibrational spectra at 6 μm have been detected and analyzed for the first time. The spectral and the subsequent structural analyses, in conjunction with the corresponding *ab initio* calculation, indicate that the OCS–NH_3 complex assumes C_{3v} symmetry with S pointing to N of NH_3, in contrast to the T-shaped geometries obtained for the isoelectronic N_2O–NH_3 and CO_2–NH_3 complexes.

1 Introduction

Inter(intra) molecular interactions govern the physical and biological properties of matter. One of the strongest and most important types of interactions is the X–H···Y hydrogen bond, in which the electropositive H atom bonded with the more electronegative X species is attracted to electron rich Y (typically a nitrogen, oxygen, or fluorine atom) of another molecule or at another site of the same molecule.[1] Although the interaction may consist of contributions from electrostatic interactions, polarization or induction interactions, dispersion, charge transfer induced covalency, and exchange correlation effects,[2–4] electrostatic interactions between electric dipoles are often a major component, distinctively characterized by its linear directionality. Vibrational spectroscopy has been an important method to study hydrogen bonds.[5–9] Usually the vibrational band corresponding to the X–H stretch gets broader, gains intensity, and is red shifted upon formation of an X–H···Y hydrogen bond. High resolution infrared spectroscopy can reveal detailed information about weakly bound complexes and the nature of the intermolecular interactions.[10–15] But there are relatively few experimental high resolution spectroscopic studies of the C–H···Y weak hydrogen bonds,[16] which have been identified in a large number of crystallographic data[17] and a few gas phase studies. Most of these studies had been concentrated on complexes with subunits that have large permanent electric dipole moments and the C–H bond connecting to strong electronegative species, such as in $(CH_3)_2O\cdots HCF_3$,[18] $C_6H_5F\cdots HCF_3$,[19] and $C_6H_5F\cdots HCCl_3$.[20] In these complexes, the C–H bond length decreases upon complexation, leading to the unusual blue-shifted C–H stretching frequency that gives name to the interactions in such complexes as "improper hydrogen bonds".[21] More recently, a unified explanation was developed for red-, blue- and non-shifting hydrogen bonds[22] where it was shown that the optimum C–H bond length in the complex can be longer, shorter or equal to that in the free monomer. Indeed, weakly hydrogen bonded complexes with red shifted C–H stretching frequencies have also been reported, *e.g.*, the $Cl_3CH\cdots NH_3$ complex.[23] Besides these strongly dipolar systems mentioned above, it is of significant interest to study the C–H···Y weak hydrogen bond consisting of a non-polar partner.

Department of Chemistry, University of Alberta, Edmonton, Canada T6G 2G2. E-mail: yunjie.xu@ualberta.ca; Fax: +1 780-492-8231; Tel: +1 780-492-1244

† Electronic supplementary information (ESI) available. See DOI: 10.1039/c1cp21554j

One such model system is the acetylene–ammonia (HCCH–NH_3) complex. The rotational spectrum of HCCH–NH_3 had been studied by Fraser *et al.*,[24] and the high resolution infrared spectrum in the vicinity of the C–H stretching vibration had also been measured.[25] These studies indicate that HCCH–NH_3 is a C_{3v} symmetric top complex with a C–H$\cdots$N weak hydrogen bond. Although there had been previous attempts to detect the infrared spectrum of this complex in the 6 μm region of ammonia *E*-symmetry ν_4 deformation, no spectral feature had been conclusively identified.[26,27]

The carbonyl sulfide–ammonia (OCS–NH_3) complex also consists of ammonia with a linear molecule, but with a permanent dipole moment. Modest resolution infrared spectra of this complex had been measured at 10 μm upon excitation of the OCS $2\nu_2$ bending overtone and the NH_3 ν_2 umbrella motion.[28] Both bands display homogeneous broadening due to photodissociation. No detailed spectroscopic assignments had been reported and therefore no direct structural information had been obtained. Microwave spectroscopic studies of the isoelectronic complexes, CO_2–NH_3 and N_2O–NH_3, showed that these complexes are T-shaped, with N of NH_3 pointing to the middle atom of the linear subunit.[28] The authors speculated that OCS–NH_3 may have a T-shaped structure as well. On the other hand, one may argue that with a much larger dipole moment (0.7 Debye) compared to N_2O (0.2 Debye) and CO_2 (no permanent dipole), it is feasible for OCS to bind to NH_3 through an electric dipole–dipole interaction and form a C_{3v} symmetric structure with the S atom pointing to ammonia, similar to that of the HCCH–NH_3 complex. So far, no microwave or high resolution infrared spectroscopic study had been reported for this complex to support either one of the proposed structures. Therefore, the OCS–NH_3 complex which has a larger dipolar subunit will provide interesting comparisons to the weak hydrogen bonded HCCH–NH_3 and the van der Waals N_2O–NH_3 and CO_2–NH_3 complexes.

In the following, we report the combined high resolution infrared and microwave spectroscopic studies and *ab initio* calculations of the HCCH–NH_3 and OCS–NH_3 complexes. The ν_4 mode of NH_3 was chosen in the current study since NH_3 is the common binding partner in these two complexes. Furthermore, it would also be interesting to compare the degree of predissociation caused by the excitation of the (bonded) ν_4 band of NH_3 (perpendicular band) *versus* the excitation of the (bonded) C–H stretch (parallel band) in the HCCH–NH_3 complex, where significant intramolecular vibrational redistribution (IVR) predissociation line broadening was reported in the latter case.[25] From the spectral and subsequent structural analyses, together with the associated *ab initio* calculations, the structures and the nature of the intermolecular forces at play in these two prototype complexes have been investigated in detail.

2 Microwave and infrared experiments

The HCCH–NH_3 and OCS–NH_3 complexes were generated in a supersonic jet expansion with 0.5% of HCCH or OCS and 0.5% of NH_3 mixture in helium (Praxair) backing gas at room temperature. For the microwave measurements, a pulsed molecular beam Fourier transform microwave spectrometer was used to measure the rotational transitions of both complexes between 5 and 18 GHz.[29] The full line width at half maximum (FWHM) of a well resolved peak is about 30 kHz and the corresponding uncertainty is estimated to be around 2 kHz. The sample gas with a stagnation pressure around 4 bar was expanded through a General Valve (Series 9) pulsed nozzle of 0.8 mm orifice diameter. For the infrared measurements, a pulsed slit-jet multipass absorption spectrometer with an external-cavity quantum cascade laser (Daylight Solutions, CW-MHF) was used to record the ro-vibrational transition of the complexes at 6 μm. The spectrometer had been built recently and described in detail and compared with an off-axis cavity enhanced absorption configuration elsewhere.[30,31] Briefly, the sample gas with a stagnation pressure around 10 bar was expanded through a homemade pulsed slit-jet nozzle with a 40 mm $\times$ 0.04 mm slit. The astigmatic multipass absorption cell was aligned with the 366-pass configuration. The infrared beam passed through the slit jet roughly parallel to the slit and was then focused onto an MCT detector after exiting the vacuum chamber. The external-cavity quantum cascade laser centered at 6 μm was swept by PZT elements using a sine voltage wave with a frequency of 100 kHz and an amplitude of 100 V, corresponding to roughly 1.5 cm^{-1} frequency coverage in each sweep. The full frequency coverage of the laser is from 1634 to 1680 cm^{-1}. The etalon channel and the reference channel which consisted of dilute NH_3 and H_2O in a Herriott multipass cell were recorded simultaneously. From sweep to sweep, a significant frequency drift was noted. This drift resulted in substantial peak broadening. To overcome this problem, each sweep was frequency calibrated using the etalon fringes and the reference gas transitions before co-adding. The instrumental line width of a well resolved peak is around 0.0015 cm^{-1}, limited by the Doppler broadening from the jet expansion.

3 Results

3.1 *Ab initio* calculations

To aid and to complement the spectroscopic study, *ab initio* calculations using the Gaussian03 program[32] have been performed for both the C_{3v} symmetric and T-shaped conformers, as well as the NH$\cdots$O and O$\cdots$N binding pairs of OCS–NH_3. The NH$\cdots$O and O$\cdots$N conformers were found to be much less stable. In fact, they are not minima at the MP2 level of theory and were not further considered. Equilibrium geometries for both C_{3v} symmetric and T-shaped conformers of OCS–NH_3 have been obtained at the MP2/aug-cc-pVTZ level of theory. (An)harmonic frequency calculations have also been performed to obtain the spectroscopic constants and vibrational frequencies. Although a theoretical study of HCCH–NH_3 with emphasis on the dissociation energy had been reported previously,[33] we have also performed the parallel *ab initio* calculations for HCCH–NH_3 for comparison. The corresponding spectroscopic constants, harmonic and anharmonic frequencies of the NH_3 ν_4 band, and dissociation energies with basis set super position errors (BSSEs)[34] and zero-point energy corrections (ZPE) have been calculated and are summarized in Table 1. The harmonic and anharmonic frequencies calculated for all the complexes and the ammonia subunit are provided in the ESI,† as well as the harmonic frequencies for the linear subunits.

Table 1 *Ab initio* equilibrium structures, dissociation energies (ΔE_0), harmonic (ν_{har}) and anharmonic (ν_{anh}) frequencies of NH_3 ν_4 deformation, and spectroscopic constants of HCCH–NH_3 and of the C_{3v} symmetric and T-shaped conformers of OCS–NH_3

	HCCH–NH_3	C_{3v} symmetric OCS–NH_3	T-shaped OCS–NH_3	
ΔE_0 MP2/aug-cc-pVTZ(raw) (kJ mol^{-1})	16.5	10.0	8.2	
ΔE_0 MP2/aug-cc-pVTZ(BSSE) (kJ mol^{-1})	14.6	8.8	7.0	
ΔE_0 MP2/aug-cc-pVTZ(BSSE + har-ZPE) (kJ mol^{-1})	9.2	6.4	4.8	
ΔE_0 CCSD(T)/6-311 + G(3df,2p)(BSSE + scaled-har-ZPE)[a] (kJ mol^{-1})	9.3	n/a	n/a	
ΔE_0 CCSD(T)/av5z′(BSSE)[b] (kJ mol^{-1})	15.1	n/a	n/a	
ΔE_0 CCSD(T)/av5z′(BSSE + har-ZPE)[b] (kJ mol^{-1})	10.2	n/a	n/a	
ν_{har}/cm^{-1}	1669.1	1668.6	1666.6	1669.5[d]
ν_{anh}[c]/cm^{-1}	1627.0	1621.8	1615.9	1627.0
ν'_{anh}[c]/cm^{-1}	1627.7	1622.2	n/a	n/a
A_0/MHz	195 782	200 748	7045	
B_0/MHz	2728	1494	2914	
C_0/MHz	n/a	n/a	2079	
D_J/kHz	5.12	1.50	18	
D_{JK}/kHz	509	474	25	
$A_{v=1}$/MHz	199 877	209 602	7305	7397
$B_{v=1}$/MHz	2669	1485	2955	2959
$C_{v=1}$[c]/MHz	2668	1484	2120	2129

[a] Ref. 33. [b] Ref. 26. [c] Anharmonicity lifts the degeneracy of the excited NH_3 ν_4 deformation, as pointed out by Oka.[35] [d] The T-shaped conformer is an asymmetric top, thus has non-degenerate NH_3 ν_4 modes and non-equal B and C rotational constants.

3.2 The HCCH–NH_3 complex

We assume the band origin of the ν_4 E-symmetry deformation of the NH_3 monomer to be 1626.825(2) cm^{-1}, which is the average of its two ν_4 fundamentals centered at 1626.276(1) cm^{-1} ($s \leftarrow s$) and 1627.375(2) cm^{-1} ($a \leftarrow a$), where s and a are the symmetry labels of the two inversion tunneling states.[36] The umbrella tunnelling motion of NH_3 in the complex is expected to be quenched because of the weak hydrogen bonding. Indeed, no tunnelling splitting was observed in the previous high resolution infrared study at 3 μm.[25] Based on the anharmonic frequency calculations of the NH_3 monomer and the HCCH–NH_3 complex, one expects the NH_3 ν_4 band to be blue shifted by ~5 cm^{-1} when NH_3 binds to HCCH through a weak C–H···N hydrogen bond. In the initial search from 1634 cm^{-1} to 1680 cm^{-1}, the full frequency region covered by the current quantum cascade laser, only one infrared band was observed. This is shown in Fig. 1. This band was confirmed to belong to HCCH–NH_3 by omitting either HCCH or NH_3 from the sample mixture. Since the transition dipole moment of NH_3 ν_4 deformation is perpendicular to the a-axis of HCCH–NH_3, one expects to see a perpendicular band. Indeed, the band observed is consistent with a typical symmetric top perpendicular band. A closer examination reveals that $R(0)$, $P(1)$, $P(2)$ transitions ($\Delta J(J'')$) are missing. Therefore this band was assigned to the $K = 2 \leftarrow 1$ subband. The frequencies of the observed transitions are listed in Table 2 in the ESI.†

As the rotational constant, A, was estimated to be about 6.5 cm^{-1} from the *ab initio* calculation, one would expect the $K = 1$ levels not to be substantially populated in a jet expansion in general. The observation of the $K = 2 \leftarrow 1$ subband is a consequence of nuclear spin statistics. Since HCCH–NH_3 is of C_{3v} symmetry with three identical hydrogen nuclei, the $K = 0$ and $K = 1$ levels are associated with A and E spin functions, respectively, with a 1 : 1 spin statistical weight ratio. In the jet expansion, the metastable $K = 1$ levels cool down separately from the $K = 0$ levels. As a result, the $K = 2 \leftarrow 1$ subband is of similar intensity as that of the $K = 1 \leftarrow 0$ subband.

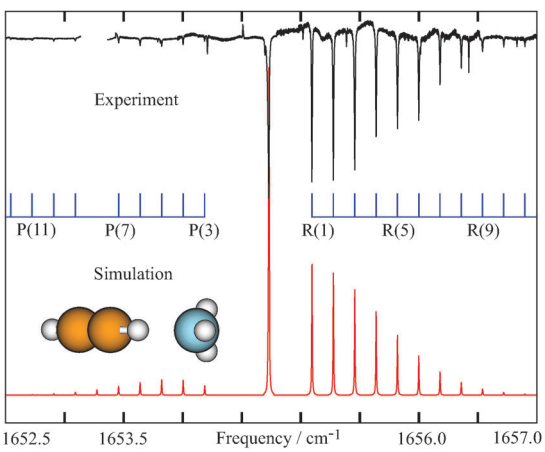

Fig. 1 Experimental high resolution infrared spectrum of HCCH–NH_3, with the calculated spectrum based on the constants in Table 2. The spectrum consists of several frequency scans. Each scan has 50 averaging sweeps to increase the signal-to-noise ratio. The gap around the $P(8)$ transition was due to a strong ammonia peak.

The corresponding a-type prolate top microwave transitions of HCCH–NH_3 had been reported previously, with K up to 1 and J up to 2.[24] We extended the measurements with K up to 2 and J up to 3. Since the $K = 0$ and $K = 1$ levels are equally populated because of the spin statistics, the ^{14}N nuclear

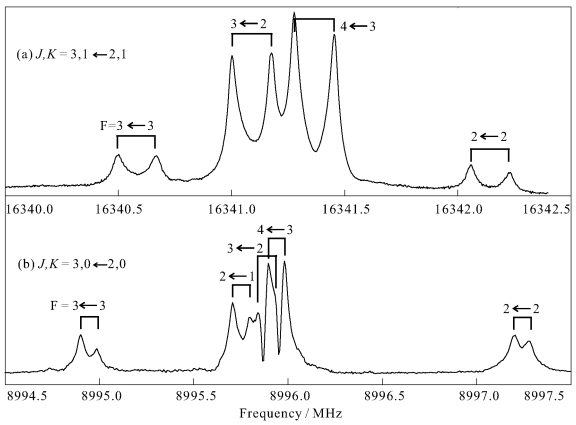

Fig. 2 Observed composite FTMW spectrum of (a) $J,K = 3,1 \leftarrow 2,1$ transition of HCCH–NH_3 and (b) $J,K = 3,0 \leftarrow 2,0$ transition of OCS–NH_3 with the ^{14}N nuclear quadrupole hyperfine structures. Each line consists of two Doppler components resulting from a molecular expansion parallel to the MW cavity axis. The $F = 2 \leftarrow 1$ component of HCCH–NH_3 is buried under the center profile.

quadrupole hyperfine structures of $K = 0$ and $K = 1$ transitions are of similar intensity. The $K = 2$ transitions, which are also associated with the *E*-symmetry spin function, were observed with much less intensity because of collisional relaxation to the $K = 1$ levels. We also re-measured all previously reported transitions for consistency. The experimental microwave transitions with ^{14}N nuclear hyperfine splitting are listed in Table 3 in the ESI†, together with the difference between the observed and calculated frequencies. The ^{14}N nuclear hyperfine components of the $J,K = 3,1 \leftarrow 2,1$ transition are depicted in Fig. 2(a). The rotational transitions were fitted with a standard semirigid symmetric top Hamiltonian using Pickett's SPFIT program.[37] The resulting spectroscopic constants are listed in Table 2. The constants obtained are very close to those reported previously, except that two sextic centrifugal distortion constants are needed because $K = 2$ transitions are also included in the fit.

Finally, the ro-vibrational transitions were fitted to the standard symmetric top Hamiltonian for a perpendicular band. The constants determined are given in Table 2. The *B* rotational constant of the excited state is essentially the same as that of the ground state while the centrifugal distortion constant D_J increases, indicating that the geometry of the complex remains basically unchanged while the C–H···N hydrogen bond gets weaker upon the ν_4 excitation.

It is worthy to point out that the doubly degenerate excited vibrational levels of a perpendicular band of a symmetric top molecule are split by a large first-order Coriolis interaction which shifts the band origin of the $K + 1 \leftarrow K$ subband to:[38]

$$\nu = \nu_0 + [A'(1 - 2\zeta) - B'] + 2[A'(1 - \zeta) - B']K + [(A' - B') - (A'' - B'')]K^2 \quad (1)$$

where ν is the subband origin and ζ is the first-order Coriolis coupling constant. Since only one subband was detected in this study, we were not able to determine ζ and *A* values experimentally. The *K*-subbands are separated by roughly $2[A(1 - \zeta) - B]$, assuming that the rotational constants of the ground and excited vibrational states are the same. The $K = 2 \leftarrow 1$ subband origin is roughly $3[A(1 - \zeta) - B] - A\zeta$ higher in frequency than the actual band origin. One would then expect to observe a strong $K = 1 \leftarrow 0$ subband at $2[A(1 - \zeta) - B]$ to the red of the observed $K = 2 \leftarrow 1$ subband. Such a band was not observed within the spectral coverage available down to 1634 cm^{-1}, indicating that $2[A(1 - \zeta) - B] > 21$ cm^{-1} or $A(1 - \zeta) > 10.6$ cm^{-1}, with the *B* value taken from the spectroscopic fit. Assuming that *A* is 6.5 cm^{-1} from the *ab initio* calculation, the ζ value is determined to be less than -0.63. Then the band origin of the ν_4 band of HCCH–NH_3 is expected to be lower than 1619.4 cm^{-1}, which is red shifted from the ammonia monomer fundamental at 1626.825(2) cm^{-1}.[36] A simulated spectrum using the PGOPHER program[39] is also shown in Fig. 1. The much greater intensity observed for the *R versus* the *P* branch has also been reproduced. This intensity pattern results from the Hönl–London factor for the vibrational band of a symmetric top rotor at the very low rotational temperature achieved in the jet expansion.

Table 2 Experimental spectroscopic constants of the vibrational ground and excited states of HCCH–NH_3 and OCS–NH_3

	ν_0	$\nu_4 = 1$
HCCH–NH_3		$K = 2 \leftarrow 1$
ν/cm^{-1}	0.0	1654.73187(18)
B_0/MHz	2724.56591(41)[a]	2724.93(16)
D_J/kHz	7.005(26)	10.97(92)
D_{JK}/kHz	895.93(63)	895.93[b]
H_{JK}/Hz	758(73)	758[b]
H_{KJ}/Hz	111(41)	111[b]
eQq^N_{aa}/MHz	−3.1302(19)	
OCS–NH_3		$K = 1 \leftarrow 0$
ν/cm^{-1}	0.0	1637.56882(16)
B_0/MHz	1499.34925(19)	1499.021(73)
D_J/kHz	1.8715(37)	1.8715[b]
D_{JK}/kHz	425.46(15)	425.46[b]
eQq^N_{aa}/MHz	−2.9751(29)	

[a] The numbers in parentheses are standard deviations in units of the last digits (1σ). [b] Fixed at the corresponding vibrational ground state value.

3.3 The OCS–NH_3 complex

No high resolution spectroscopic study of the OCS–NH_3 complex had been reported previously. The C_{3v} symmetric and T-shaped conformers of OCS–NH_3 were predicted to have only a small energy difference, with the C_{3v} symmetric conformer being slightly more stable. It is therefore not known *a priori* which conformer or whether both of them will be detected experimentally. Although the whole available quantum cascade laser frequency region from 1634 cm^{-1} to 1680 cm^{-1} was scanned very carefully for any vibrational band due to OCS–NH_3, only one weak band centered at 1637.6 cm^{-1} was detected. This is depicted in Fig. 3. The band shows a perpendicular band pattern with a strong Q-branch bandhead. Its intensity is considerably weaker than that of the $K = 2 \leftarrow 1$ subband of HCCH–NH_3 described above. Furthermore, the lines observed show much more severe predissociation broadening than those observed in the HCCH–NH_3 complex.

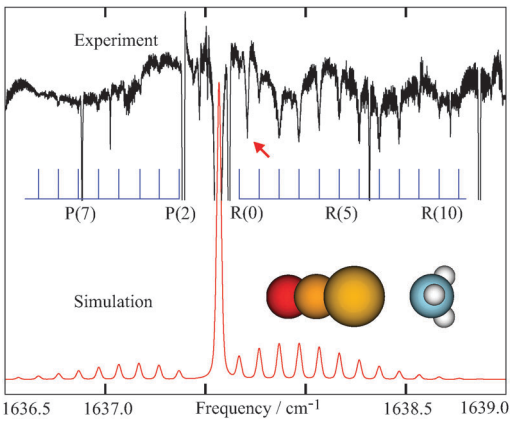

Fig. 3 Observed infrared spectrum of OCS–NH_3 at 6 μm, together with the corresponding simulated spectrum using the PGOPHER program. The spectrum consists of several scans and each scan is averaged with 50 sweeps. The several strong transitions with a line width of $\sim$0.015 cm^{-1} are due to the NH_3 monomer. The broad peak at 1637.709 cm^{-1} (marked with an arrow) is unassigned. See further discussions in the text.

This band was tentatively assigned to the C_{3v} symmetric conformer based on the predicted rotational constants and transition dipole moment. The NH_3 ν_4 band of the T-shaped conformer, on the other hand, was predicted to have a much different vibrational spectral pattern. It was further assigned to the $K = 1 \leftarrow 0$ subband because the $P(1)$, $P(2)$, and $R(0)$ transitions are all present in the spectrum. Applying the same spin statistical consideration for OCS–NH_3 as for HCCH–NH_3 discussed above, one expects to detect the $K = 2 \leftarrow 1$ subband of similar intensity at the higher frequency region. This was, however, not observed in our laser frequency coverage up to 1680 cm^{-1}. This might be due to a large $2[A(1-\zeta) - B]$ spacing between the two subbands. Since the intensity of the $K = 1 \leftarrow 0$ subband is very weak, it is also likely that the $K = 2 \leftarrow 1$ subband may simply be too weak to be detected with the sensitivity of the current spectrometer.

In the preliminary spectroscopic analysis, the observed infrared transitions were fitted to a symmetric top rotor Hamiltonian with the rotational constants of the ground and excited vibrational states kept the same. The search for the microwave transitions was guided using the experimental B constant obtained from the preliminary analysis. The a-type pure rotational transitions were identified straightforwardly, with the characteristic ^{14}N nuclear quadrupole hyperfine structure. The detected rotational transitions with J up to 5 are listed in Table 3 of the ESI.† The ^{14}N nuclear hyperfine structure of $J,K = 3,0 \leftarrow 2,0$ transition is shown in Fig. 2(b). Consistent with the infrared study, the intensity of the microwave transitions of OCS–NH_3 is much weaker than that of HCCH–NH_3. The rotational transitions were fitted with a standard semirigid symmetric top Hamiltonian, including the ^{14}N nuclear quadrupole coupling term. The current rotational study therefore confirmed the assignment of the rovibrational transitions proposed above. The observed rovibrational transitions were then fitted with a standard semirigid rotor Hamiltonian for a perpendicular band. The spectroscopic constants obtained are listed in Table 1. It is noticed that the B rotational constant changes 0.022% upon ν_4 excitation in OCS–NH_3, compared to 0.013% in HCCH–NH_3. It was noted that the experimental intensity observed for HCCH–NH_3 was much stronger than that of OCS–NH_3 in our microwave experiments. A similar phenomenon was observed for the infrared measurements. We attributed this to fewer OCS–NH_3 made in the jet expansion than that of HCCH–NH_3.

As mentioned before, the T-shaped conformer was predicted to be less stable than the observed C_{3v} symmetric conformer by only 1.6 kJ mol^{-1}. In the recorded infrared spectrum (see Fig. 3), besides the symmetric top OCS–NH_3 subband, the rest of the peaks are transitions of the NH_3 monomer, except the broad peak at 1637.709 cm^{-1}. We initially speculated that the T-shaped OCS–NH_3 might be the carrier for this unassigned broad peak. However, no corresponding transitions of the T-shaped conformer were found in the microwave spectrum. The failure to detect the T-shaped conformer confirms the *ab initio* prediction that the symmetric top conformer is more stable.

4 Discussions

4.1 Structure and dynamics

Both the infrared and microwave spectra measured are consistent with the C_{3v} symmetric structures of the HCCH–NH_3 and OCS–NH_3 complexes. The spectroscopic constants obtained allow us to carry out structural analyses,[24,40] assuming that there is no distortion of the subunits upon complexation. For the structures of the complexes, five additional degrees of freedom are needed to describe the relative orientation and separation of the two subunits, as illustrated in Fig. 4.

The value of χ can be estimated from the measured quadrupole coupling constants eQq_{aa}^{N} by assuming that the electric field gradient at the nitrogen nucleus doesn't change upon complexation:

$$eQq_{aa}^{N} = eQq_{NH_3}^{N}\langle P_2(\cos\chi)\rangle = eQq_{NH_3}^{N}\left(\frac{3\langle\cos^2\chi\rangle - 1}{2}\right) \quad (2)$$

With the value of $eQq_{NH_3}^{N} = -4.089$ MHz taken from the NH_3 monomer,[41] χ is determined to be 23.29(2)° and 25.23(4)° for

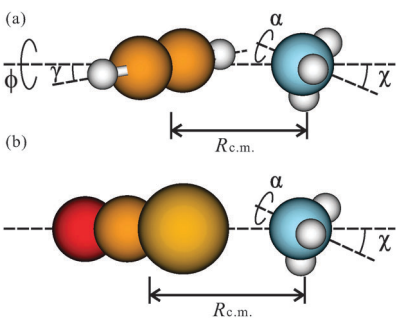

Fig. 4 Definition of coordinates used to describe the structure of (a) HCCH–NH_3 and (b) OCS–NH_3. The distance between the centers of mass of the two subunits is $R_{c.m.}$. The motions of the NH_3 and HCCH subunits with respect to the a-axis of the complex are described by the cones traced out by their highest symmetry axes with an averaged angle of χ and γ, respectively. Their relative orientation is specified by ϕ. For the OCS–NH_3 complex, γ is set to zero. The rotation of NH_3 along its C_3 axis is described by angle α.

HCCH–NH_3 and OCS–NH_3, respectively. For comparison, χ is 20.4° for the HCN–NH_3 complex with a strong hydrogen bond.[42] The magnitude of χ can be correlated to the binding strength of the complex. Stronger binding interactions between ammonia and HCN and between ammonia and HCCH result in smaller χ values, and therefore smaller vibrational amplitudes of NH_3. The χ values mentioned above are consistent with the binding strength order: HCN–NH_3 > HCCH–NH_3 > OCS–NH_3. Similarly, the angle γ specifies the average vibrational amplitude of the HCCH or OCS subunit with respect to the *a*-axis of the corresponding complex. Since these subunits contain no quadrupolar nucleus, we are not able to apply the same method to obtain the γ value. For the HCCH–NH_3 complex, this angle can be assumed to have the same value as in the HCN–NH_3 complex[42] since these two complexes have similar C–H···N hydrogen bonds and the masses of the HCCH and HCN subunits are essentially the same. For the much heavier OCS subunit in the OCS–NH_3 complex, the angle γ can be expected to be much smaller and was fixed to zero in the following structural analyses.[43]

The moments of inertia for the complex consist of the contribution from the end-over-end pseudo-diatomic rotation of the complex and those from the two subunits. For the HCCH–NH_3 complex:

$$I_b = \mu_R \langle R_{c.m.}^2 \rangle + I_b^{NH_3}\left(\frac{1+\langle\cos^2\chi\rangle}{2}\right) + I_c^{NH_3}\left(\frac{\langle\sin^2\chi\rangle}{2}\right) + I_b^{C_2H_2}\left(\frac{1+\langle\cos^2\gamma\rangle}{2}\right) \quad (3)$$

where μ_R is the reduced mass of the two subunits and $I_b^{NH_3}$, $I_c^{NH_3}$, and $I_b^{C_2H_2}$ are the effective principle moments of inertia of NH_3 and HCCH, taken from the free monomer values.[44,45] The separation of the centers of mass of HCCH and NH_3 ($R_{c.m.}$) was calculated to be 4.0594(6) Å. Similarly, $R_{c.m.}$ in OCS–NH_3 was calculated to be 4.3607(2) Å for the OCS–NH_3 complex, with the γ value fixed to zero and the moment of inertia of the OCS monomer taken from the free monomer value.[46,47] With the structural parameters of HCCH and OCS fixed at their respective experimental values of the corresponding monomers,[48,49] the C–H···N hydrogen bond length ($R_{H\cdots N}$) and the S···N bond length ($R_{S\cdots N}$) have been determined to be 2.3980(7) Å and 3.3233(2) Å, respectively. Considering the excited vibrational state, the *B* rotational constant varies very little upon ν_4 excitation of NH_3 in both complexes, suggesting that the bending excitation has minimal influence on the structures of these complexes. A similar phenomenon has also been found in a number of other complexes, for example, the ν_2 bending excitation of water in Ar–H_2O.[50] All of the structural parameters determined from spectroscopic constants are listed in Table 3. The errors indicated are purely from the uncertainties of the experimental spectroscopic constants, without taking into account the approximation made.

The ro-vibrational transitions detected for both HCCH–NH_3 and OCS–NH_3 have notable homogeneous broadening. This is likely due to vibrational predissociation where the excitation of ν_4 vibration of NH_3 is coupled to the excitation of the intermolecular stretching mode C–H···N or S···N, leading to the dissociation of the complex. For a well resolved transition measured with the same laser spectrometer without any lifetime broadening, the typical FWHM fitted with a Gaussian line shape was 0.0015 cm^{-1}.[31] The broadening due to vibrational predissociation has been estimated with a Lorentzian line shape to be 0.005 cm^{-1} (FWHM) for HCCH–NH_3 and 0.01 cm^{-1} (FWHM) for OCS–NH_3, respectively. The expression $\tau = 1/(2\pi\Gamma)$, where Γ is the Lorentzian FWHM, leads to a rough estimation of 1 ns and 0.5 ns for the excited states lifetime for HCCH–NH_3 and OCS–NH_3, respectively.

Table 3 Experimental structural parameters and dissociation energies of HCCH–NH_3 and OCS–NH_3

	HCCH–NH_3	OCS–NH_3
χ/°	23.29(2)	25.23(4)
$R_{c.m.}$/Å	4.0594(6)	4.3607(2)
$R_{H/S\cdots N}$/Å	2.3980(7)	3.3233(2)
k_s/N m^{-1}	7.12(3)	4.687(9)
ν_s/cm^{-1}	108.3(2)	77.45(7)
ΔE_0^a/kJ mol^{-1}	9.81(4)	7.46(1)

[a] Lennard-Jones potential was assumed to obtain the dissociation energy value. See text and Fig. 4 for definition of these parameters.

More severe predissociation broadening had been reported for HCCH–NH_3 when the bonded C–H stretching mode was excited.[25] The stronger coupling of the bonded C–H stretch than the NH_3 deformation to the intermolecular H···N stretching mode is reasonable since the transition dipole moment of the former is aligned with that of the intermolecular stretching mode, whereas that of the latter is perpendicular to it. The stronger coupling of the ν_4 excitation of NH_3 to the S···N stretch in OCS–NH_3 is difficult to rationalize. Although the shorter predissociation life time was observed for OCS–NH_3 than for HCCH–NH_3, it may not be too meaningful to discuss this small difference because the two complexes have very different well depths and different masses of the coupling atom. Nevertheless, if such vibrational coupling depends strongly on the electric dipole–dipole interaction, one may propose that the possible cause is the larger dipole moment of OCS (0.7 Debye), as compared to the non-polar HCCH. But the previous study[25] of the predissociation lifetimes of HCCH–NH_3, HCN–NH_3, and HCCH–H_2O[51] shows that HCCH–NH_3 has a much broader predissociation line width than the other two, even though the dipole moment of ammonia (1.5 Debye) is less than that of water (1.9 Debye), and HCCH is non-polar. Further studies of other related systems would be desirable to allow more concrete discussions.

4.2 Dissociation energies

The van der Waals (vdw) stretching force constant (k_s) of the complex could be estimated using the pseudo-diatomic approximation:[52]

$$k_s = \frac{\hbar^4 \mu_R}{2 D_J h} \frac{I_{AB} - I_A - I_B}{I_{AB}^4} \quad (4)$$

where D_J is the centrifugal distortion constant. I_{AB}, I_A, and I_B are the principle *b*-inertial moments of the AB complex and the

A and B monomers, respectively. The experimental effective principle moments of inertia were used for the subunits and the complex. With eqn (4), the stretching force constants for HCCH–NH_3 and OCS–NH_3 were calculated to be 7.12(3) and 4.687(9) N m^{-1}, respectively, corresponding to the harmonic ($\sqrt{k/\mu}$) vdW vibrational frequencies of 108.3(2) cm^{-1} and 77.45(7) cm^{-1}, respectively. If a Lennard-Jones type potential was assumed, the dissociation energy (ΔE_0) could be estimated with the following equation:[53]

$$\Delta E_0 = \frac{1}{72} k_s R_{c.m.}^2 \quad (5)$$

ΔE_0 of 9.81(4) kJ mol^{-1} and 7.46(1) kJ mol^{-1} were obtained for the HCCH–NH_3 and OCS–NH_3 complexes, respectively. The errors indicated are from the uncertainties of the experimental spectroscopic constants. It is difficult to provide an exact uncertainty of this derived value compared to the true value which is rarely available. This uncertainty is most likely to be system dependent, *i.e.*, how closely the Lennard-Jones potential resembles the true potential in each case. Judging from the general good agreement with the high level *ab initio* calculation, one can cautiously say that the uncertainty is probably within 1 kJ mol^{-1}. Inclusion of the harmonic zero-point energies (har-ZPE) further improves the agreement between the experimental and calculated values. The har-ZPE corrected values appear to be overcorrect in the present cases, although one should keep in mind that the absolute uncertainty of the experimental values is about 1 kJ mol^{-1} as discussed above.

The noticeable larger dissociation energy of HCCH–NH_3 compared to that of OCS–NH_3 highlights the strength of a C–H$\cdots$N weak hydrogen bond, even though it is comparatively weaker than the O–H$\cdots$N or N–H$\cdots$N bond. It is known that in these neutral complexes, the electrostatic interactions are often the driving force for the orientation preference exhibited by a particular complex. Assuming simple dipole–quadrupole and quadrupole–quadrupole interactions at the corresponding center-of-mass distances, one can obtain the attractive electrostatic interaction energies of 0.7 and 11.0 kJ mol^{-1} for the T-shaped and the C_{3v} symmetric HCCH$\cdots$$NH_3$, respectively. Clearly, electrostatic interaction plays an important role in the C_{3v} symmetric preference of HCCH$\cdots$$NH_3$. Similarly, the electrostatic interaction energies for the C_{3v} symmetric and T-shaped OCS$\cdots$$NH_3$ were calculated to be 1.6 and 0.4 kJ mol^{-1}. Calculation details are provided in the ESI.† The much stronger electrostatic interaction in HCCH$\cdots$$NH_3$ *versus* that in OCS$\cdots$$NH_3$ can also be visualized in terms of the electrostatic potentials mapped on the electron density isosurface obtained from the *ab initio* calculations. As one can see, the attractive field strength experienced by the N atom of ammonia in HCCH$\cdots$$NH_3$ is considerably larger than in OCS$\cdots$$NH_3$ (see Fig. S1 of the ESI†). Furthermore, the preference for a C_{3v} symmetric instead of a T-shaped orientation in OCS$\cdots$$NH_3$ can also be visualized in terms of the attractive field strength experienced by the N atom of ammonia as shown in Fig. S2 of the ESI†, although the preference here is quite subtle.

We would also like to point out that the harmonic frequency calculations reported above predict a red shift of the bonded C–H stretch by 96 cm^{-1}, in reasonable agreement with the experimental value of 75.1042(38) cm^{-1}.[25] A recent report on $Cl_3CH\cdots NH_3$ also showed that the shift in the C–H stretch was well reproduced at the harmonic level.[23] Unfortunately, the limited laser frequency coverage prevents us from obtaining the experimental shifts of the ν_4 NH_3 band in the two complexes to make the similar comparisons with the calculations.

It is of interest to compare the most stable structures of the isoelectronic OCS–NH_3, N_2O–NH_3 and CO_2–NH_3 complexes. While OCS–NH_3 is a C_{3v} symmetric top with an S$\cdots$N intermolecular bond, the latter two have a T-shaped structure with N of ammonia pointing to the middle atom of the linear molecule. This is because the much larger electric dipole moment of OCS results in a strong electric dipole–dipole interaction with NH_3, favoring the symmetric top structure. For N_2O and CO_2, which have small or zero electric dipole moments, the interactions with NH_3 are dominated by the induction and London dispersion forces.[54] A similar structural trend had been reported for the corresponding complexes with water. For example, the OCS–H_2O[43] complex displays a similar "linear" conformation with the electropositive sulfur binding to the negative oxygen of water, while CO_2–H_2O[55] and N_2O–H_2O[56] are T-shaped.

5 Conclusions

Pure rotational spectra and rovibrational spectra at 6 μm of the HCCH–NH_3 and OCS–NH_3 complexes have been detected and analyzed. The structures of both complexes have been determined to be of C_{3v} symmetry. The quadrupolar acetylene binds to ammonia through a weak C–H$\cdots$N hydrogen bond and carbonyl sulfide binds to ammonia through an S$\cdots$N bond where the orientation preference is dominated by the permanent electric multipole moment interactions. The experimental dissociation energy has been found to be considerably larger for HCCH–NH_3, which highlights the strength of the comparably weak C–H$\cdots$N hydrogen bond.

Acknowledgements

This research was funded by the University of Alberta, the Natural Sciences and Engineering Research Council of Canada, the Canada Foundation for Innovation, and Alberta Ingenuity. We thank the anonymous referees for their constructive comments to improve the manuscript. We thank Dr W. Jäger for the instrument time on the microwave spectrometer and Dr F. X. Sunahori for helpful discussion. X. L. thanks Alberta Innovates for a studentship.

References

1 E. Arunan, G. R. Desiraju, R. A. Klein, J. Sadlej, S. Scheiner, I. Alkorta, D. C. Clary, R. H. Crabtree, J. J. Dannenberg, P. Hobza, H. G. Kjaergaard, A. C. Legon, B. Mennucci and D. J. Nesbitt, Definition of the Hydrogen Bond, *Pure Appl. Chem.*, 2011, DOI: 10.1351/PAC-REC-10-01-02.
2 B. Jeziorski, R. Moszynski and K. Szalewicz, *Chem. Rev.*, 1994, **94**, 1887–1930.
3 A. J. Stone, *The Theory of Intermolecular Forces*, Clarendon Press, 1997.

4 W. Gans and J. C. A. Boeyens, *Intermolecular Interactions*, Springer, 1998.
5 A. S. N. Murthy and C. N. R. Rao, *Appl. Spectrosc. Rev.*, 1968, **2**, 69.
6 J. B. Asbury, T. Steinel, C. Stromberg, K. J. Gaffney, I. R. Piletic, A. Goun and M. D. Fayer, *Phys. Rev. Lett.*, 2003, **91**, 237402.
7 J. Zheng, K. Kwak and M. D. Fayer, *Acc. Chem. Res.*, 2007, **40**, 75–83.
8 M. Banno, K. Ohta, S. Yamaguchi, S. Hirai and K. Tominaga, *Acc. Chem. Res.*, 2009, **42**, 1259–1269.
9 A. Mahjoub, A. Chakraborty, V. Lepere, K. L. Barbu-Debus, N. Guchhait and A. Zehnacker, *Phys. Chem. Chem. Phys.*, 2009, **11**, 5160.
10 R. E. Miller, *Science*, 1988, **240**, 447–453.
11 D. J. Nesbitt, *Chem. Rev.*, 1988, **88**, 843–870.
12 R. J. Saykally, *Acc. Chem. Res.*, 1989, **22**, 295–300.
13 R. E. Miller, *Acc. Chem. Res.*, 1990, **23**, 10–16.
14 D. J. Nesbitt, *Annu. Rev. Phys. Chem.*, 1994, **45**, 367–399.
15 Z. Bačić and R. E. Miller, *J. Phys. Chem.*, 1996, **100**, 12945–12959.
16 A. J. Barnes, *J. Mol. Struct.*, 2004, **704**, 3–9.
17 T. Steiner and G. R. Desiraju, *Chem. Commun.*, 1998, 891–892.
18 B. J. van der Veken, W. A. Herrebout, R. Szostak, D. N. Shchepkin, Z. Havlas and P. Hobza, *J. Am. Chem. Soc.*, 2001, **123**, 12290–12293.
19 B. Reimann, K. Buchhold, S. Vaupel, B. Brutschy, Z. Havlas, V. Špirko and P. Hobza, *J. Phys. Chem. A*, 2001, **105**, 5560–5566.
20 P. Hobza, V. Spirko, Z. Havlas, K. Buchhold, B. Reimann, H. Barth and B. Brutschy, *Chem. Phys. Lett.*, 1999, **299**, 180–186.
21 P. Hobza and Z. Havlas, *Chem. Rev.*, 2000, **100**, 4253–4264.
22 J. Joseph and E. Jemmis, *J. Am. Chem. Soc.*, 2007, **129**, 4620–4632.
23 M. Hippler, S. Hesse and M. Suhm, *Phys. Chem. Chem. Phys.*, 2010, **12**, 13555–13565.
24 G. T. Fraser, K. R. Leopold and W. Klemperer, *J. Chem. Phys.*, 1984, **80**, 1423.
25 G. Hilpert, G. T. Fraser and A. S. Pine, *J. Chem. Phys.*, 1996, **105**, 6183.
26 Y. Liu, M. A. Suhm and P. Botschwina, *Phys. Chem. Chem. Phys.*, 2004, **6**, 4642.
27 J. A. Parr, G. Li, I. Fedorov, A. J. McCaffery and H. Reisler, *J. Phys. Chem. A*, 2007, **111**, 7589–7598.
28 G. T. Fraser, D. D. Nelson, A. Charo and W. Klemperer, *J. Chem. Phys.*, 1985, **82**, 2535.
29 Y. Xu and W. Jäger, *J. Chem. Phys.*, 1997, **106**, 7968.
30 Y. Xu, X. Liu, Z. Su, R. M. Kulkarni, W. S. Tam, C. Kang, I. Leonov and L. D'Agostino, *Proceedings of SPIE*, San Jose, CA, USA, 2009, pp. 722208–722211.
31 X. Liu, Y. Xu, Z. Su, W. S. Tam and I. Leonov, *Appl. Phys. B: Lasers Opt.*, 2010, **102**, 629–639.
32 M. J. Frisch, G. W. Trucks, H. B. Schlegel, G. E. Scuseria, M. A. Robb, J. R. Cheeseman, J. A. Montgomery Jr., T. Vreven, K. N. Kudin, J. C. Burant, J. M. Millam, S. S. Iyengar, J. Tomasi, V. Barone, B. Mennucci, M. Cossi, G. Scalmani, N. Rega, G. A. Petersson, H. Nakatsuji, M. Hada, M. Ehara, K. Toyota, R. Fukuda, J. Hasegawa, M. Ishida, T. Nakajima, Y. Honda, O. Kitao, H. Nakai, M. Klene, X. Li, J. E. Knox, H. P. Hratchian, J. B. Cross, V. Bakken, C. Adamo, J. Jaramillo, R. Gomperts, R. E. Stratmann, O. Yazyev, A. J. Austin, R. Cammi, C. Pomelli, J. W. Ochterski, P. Y. Ayala, K. Morokuma, G. A. Voth, P. Salvador, J. J. Dannenberg, V. G. Zakrzewski, S. Dapprich, A. D. Daniels, M. C. Strain, O. Farkas, D. K. Malick, A. D. Rabuck, K. Raghavachari, J. B. Foresman, J. V. Ortiz, Q. Cui, A. G. Baboul, S. Clifford, J. Cioslowski, B. B. Stefanov, G. Liu, A. Liashenko, P. Piskorz, I. Komaromi, R. L. Martin, D. J. Fox, T. Keith, M. A. Al-Laham, C. Y. Peng, A. Nanayakkara, M. Challacombe, P. M. W. Gill, B. Johnson, W. Chen, M. W. Wong, C. Gonzalez and J. A. Pople, *Gaussian 03, Revision E.01*, Gaussian, Inc., Wallingford, CT, 2004.
33 M. Hartmann and L. Radom, *J. Phys. Chem. A*, 2000, **104**, 968–973.
34 S. F. Boys and F. Bernardi, *Mol. Phys.*, 1970, **19**, 553.
35 T. Oka, *J. Chem. Phys.*, 1967, **47**, 5410.
36 C. Cottaz, I. Kleiner, G. Tarrago, L. Brown, J. Margolis, R. Poynter, H. Pickett, T. Fouchet, P. Drossart and E. Lellouch, *J. Mol. Spectrosc.*, 2000, **203**, 285–309.
37 H. M. Pickett, *J. Mol. Spectrosc.*, 1991, **148**, 371–377.
38 D. Papoušek and M. R. Aliev, *Molecular Vibrational–Rotational Spectra*, Elsevier, 1982.
39 C. M. Western University of Bristol, *PGOPHER, A Program for Simulating Rotational Structure*, http://pgopher.chm.bris.ac.uk/.
40 K. Matsumura, F. J. Lovas and R. D. Suenram, *J. Mol. Spectrosc.*, 1990, **144**, 123–138.
41 M. D. Marshall and J. S. Muenter, *J. Mol. Spectrosc.*, 1981, **85**, 322–326.
42 G. T. Fraser, K. R. Leopold, D. D. Nelson, A. Tung and W. Klemperer, *J. Chem. Phys.*, 1984, **80**, 3073.
43 Y. Tatamitani and T. Ogata, *J. Chem. Phys.*, 2004, **121**, 9885.
44 Y. Kabbadj, M. Herman, G. D. Lonardo, L. Fusina and J. W. C. Johns, *J. Mol. Spectrosc.*, 1991, **150**, 535–565.
45 Š. Urban, R. D'cunha, K. N. Rao and D. Papoušek, *Can. J. Phys.*, 1984, **62**, 1775–1791.
46 S. Tranchart, I. H. Bachir, T. Huet, A. Olafsson, J. Destombes, S. Naïm and A. Fayt, *J. Mol. Spectrosc.*, 1999, **196**, 265–273.
47 M. Mürtz, P. Palm, W. Urban and A. Maki, *J. Mol. Spectrosc.*, 2000, **204**, 281–285.
48 A. Baldacci, S. Ghersetti, S. C. Hurlock and K. Narahari Rao, *J. Mol. Spectrosc.*, 1976, **59**, 116–125.
49 A. G. Maki and D. R. Johnson, *J. Mol. Spectrosc.*, 1973, **47**, 226–233.
50 M. J. Weida and D. J. Nesbitt, *J. Chem. Phys.*, 1997, **106**, 3078.
51 P. A. Block, M. D. Marshall, L. G. Pedersen and R. E. Miller, *J. Chem. Phys.*, 1992, **96**, 7321.
52 D. Millen, *Can. J. Chem.*, 1985, **63**, 1477.
53 R. P. A. Bettens, R. M. Spycher and A. Bauder, *Mol. Phys.*, 1995, **86**, 487.
54 F. London, *Z. Phys.*, 1930, **63**, 245.
55 K. I. Peterson and W. Klemperer, *J. Chem. Phys.*, 1984, **80**, 2439.
56 D. Zolandz, D. Yaron, K. I. Peterson and W. Klemperer, *J. Chem. Phys.*, 1992, **97**, 2861.